Organic Electronics 11 (2010) 1844–1852

Contents lists available at ScienceDirect

Organic Electronics

journal homepage: www.elsevier.com/locate/orgel

Deep-blue OLEDs using novel efficient spiro-type dopant materials

Young-Min Jeon [a], Jun-Yeop Lee [b], Joon-Woo Kim [c], Chil-Won Lee [c], Myoung-Seon Gong [d,*]

[a] Department of Chemistry, Dankook University, Chungnam 330-714, Republic of Korea
[b] Department of Polymer Engineering, Dankook University, Yongin, Kyung-gi 448-701, Republic of Korea
[c] OLED Team, Daejoo Electronic Materials, Siheung, Kyung-gi 429-848, Republic of Korea
[d] Department of Nanobiomedical Science and WCU Research Center of Nanobiomedical Science, Dankook University, Cheonan, Chungnam 330-714, Republic of Korea

ARTICLE INFO

Article history:
Received 31 March 2010
Received in revised form 16 May 2010
Accepted 6 August 2010
Available online 19 August 2010

Keywords:
Deep blue
Spiro[fluorene-benzofluorene]
Dopant
Color purity
OLED
Host

ABSTRACT

The deep blue fluorescent spiro-type dopant materials *N,N,N′,N′*-tetraphenylspiro[fluorene-7,9′-benzofluorene] (**SFBF**)-5,9-diamine (BD-6DPA), *N,N′*-di-(2-naphthyl)-*N,N′*-diphenyl-**SFBF**-5,9-diamine (BD-6NPA), *N,N′*-diphenyl-*N,N′*-di-*m*-tolyl-**SFBF**-5,9-diamine (BD-6MDPA) and *N,N′*-diphenyl-*N,N′*-bis(4-(trimethylsilyl)phenyl)-**SFBF**-5,9-diamine (BD-6TMSA) were designed and successfully prepared by amination reactions. The EL characteristics of MADN as the blue host material doped with the above blue dopant materials were evaluated. The electroluminescence spectra of ITO/*N,N′-diphenyl-N,N′*-bis-[4-(phenyl-*m*-tolyl-amino)-phenyl]-biphenyl-4,4′-diamine (DNTPD/*N,N′*-di(1-naphthyl)-*N,N′*-diphenylbenzidine (NPB)/2-methyl-9,10-di(2-naphthyl)anthracene (MADN):BD-6MDPA/tris(8-hydroxyquinoline)aluminum (Alq_3)/LiF/Al devices show a narrow emission band with a full width at half maximum of 48 nm and a $\lambda_{max}(\varepsilon)$ = 463 nm. The device obtained from MADN doped with BD-6MDPA showed a good color purity (0.135, 0.156), high luminance efficiency (9.11 cd/A at 6.5 V) and high external quantum efficiency (8.16%).

1. Introduction

Organic light emitting diodes (OLEDs) have attracted considerable attention due to their many advantages for commercial applications, such as their high brightness, low power consumption, capability of emitting a wide range of colors, and applications in full color organic displays [1]. For full color displays, three primary colors (red, green, blue) are necessary. Many new materials with red, green, and blue emitting colors have been developed to meet these requirements [2]. Developing blue light emitters is essential for the development of full color displays. In spite of the considerable advances that have been made in the field of OLEDs, it is difficult to find appropriate blue emitting materials because of their low solution and low solid-state photoluminescence (PL) quantum yields [3]. OLED devices have a short lifetime because of the deterioration of the luminescent layers. Their lifetimes can be lengthened by the introduction of thermally stable substituents on the host and dopant materials [4]. Generally, host and supporting layer materials having a high glass transition temperature are needed to obtain a long lifetime. Especially, the lifetime of the luminescent layers is closely related to the specific host material in use [5].

The color purity of a blue light emitter is determined by the dopant, and is improved by shifting the emission region to a shorter wavelength. The maximum emission range of some commercial dopant materials are close to the blue sky region (450–470 nm), but wavelengths lower than 450 nm are also considered to have reasonable color purity [6,7]. In addition, many problems still remain to be solved regarding durability over time due to long-term usage, and deterioration caused by oxygen and moisture in air. In addition, many other problems remain related to the need for good color purity of blue luminescence in applications such as full color displays [8].

* Corresponding author. Tel./fax: +82 41 5501476.
E-mail address: msgong@dankook.ac.kr (M.-S. Gong).

1566-1199/$ - see front matter © 2010 Elsevier B.V. All rights reserved.
doi:10.1016/j.orgel.2010.08.007

On the other hand, spiro compounds with specific steric configurations has been attracting attention as an organic functional material because of the specific physical properties of the material, such as high glass transition temperature, which makes them a very promising approach for optoelectric materials [9]. Much of the recent research into blue light-emitting materials has centered on spiro-based derivatives because of their high solution and solid-state photoluminescence quantum yields [10]. Representative organic spiro materials as blue light-emitting materials include spiro-oligophenyl [11], spirofluorenes (**SFs**) with asymmetric substitution [12],spiro-substituted **SF** [13], **SF**-linked phenylanthracene [14] and anthracene [15], heteroatom-substituted spiro compounds [16], pyrene-substituted **SFs** [17] and difluorene-indenofluorene compounds [18]. Many studies have dealt with the spiro[fluorene-7,9′-benzofluorene] (**SFBF**) as organic electroluminescent host materials. The performance of OLEDs (the color purity and luminescence efficiency) based on **SFBF** was determined by the position of substitution and aryl moieties with a variety of conjugation chain length [19].

In this study, we report the synthesis of a series of new deep-blue emitting dopant materials, *N,N,N′,N′*-tetraphenyl-**SFBF**-5,9-diamine(BD-6DPA), *N,N′*-di-(2-naphthyl)-*N,N′*-diphenyl-**SFBF**-5,9-diamine (BD-6NPA), *N,N′*-diphenyl- *N,N′*-di-*m*-tolyl-**SFBF**-5,9-diamine (BD-6MDPA) and *N,N′*-diphenyl-*N,N′*-bis(4-(trimethylsilyl)phenyl)-**SFBF**-5,9-diamine (BD-6TMSA) by amination reactions of both 5- and 9-positions on the **SFBF**. Multilayered OLEDs were fabricated by using these deep-blue materials as the emitting layer and the dopant for MADN. A high quantum efficiency of 8.16% with CIE coordinates of (0.135, 0/156) was achieved, and this is one of the best efficiency value of deep blue fluorescence OLEDs ever reported in the literature.

2. Experimental

2.1. Materials and measurements

Tetrakis(triphenylphosphine)palladium(0) and bromine (Aldrich Chem. Co.) were used without further purification. Diphenyl-[4-(2-[1,1;4,1]terphenyl-4-yl-vinyl)-phenyl]-amine (BD-1) and 2-methyl-9,10-di(2-naphthyl)anthracene (MADN) were prepared using a method reported elsewhere [22]. Tetrahydrofuran and toluene were distilled over sodium and calcium hydride. Diphenylamine, *N*-phenyl-2-naphthylamine and 3-methyldiphenylamine (Aldrich Chem. Co.) were used as received. *N*-phenyl-4-(trimethylsilyl)aniline was prepared by the literature method previously reported [23]. Tri-*t*-butylphosphine, potassium *t*-butoxide (Aldrich Chem. Co.), palladium(II) acetate (TCI Co.) were used as received for amination. 5-Bromo-**SFBF** and 5,9-bromo-**SFBF** [19] were prepared as previously reported.

The FT-IR spectra were obtained using a Biorad Excaliber FTS-3000MX spectrophotometer, and the ^{1}H NMR and ^{13}C NMR spectra were recorded on a Bruker Avance 500 (500 MHz for ^{1}H and 125 MHz for ^{13}C) spectrometer. The photoluminescence (PL) spectra were recorded on a fluorescence spectrophotometer (Jasco FP-6500) and the UV–vis spectra were obtained using a UV–vis spectrophotometer (Shimadzu, UV-1601PC). Elemental analyses were performed using a CE Instrument (EA1110), and the differential scanning calorimetry (DSC) measurements were performed using a Mettler DSC 822^{e} under nitrogen at a heating rate of 10 °C/min. The low and high resolution mass spectra were recorded using a mass spectrometer (JEOL, JMS-AX505WA) in FAB mode. The energy levels were measured using a low energy photoelectron spectrometer (Riken-Keiki AC-2). The current–voltage characteristics of the encapsulated devices were measured using a Keithley 2400 source measurement unit and CS 1000 spectroradiometer.

2.2. General procedure for the coupling reaction

The 5,9-dibromo-**SFBF** (**1**) (5 g, 9.53 mmol), diarylamine derivative (24.79 mmol) and palladium acetate (0.150 g, 0.67 mmol) were dissolved in anhydrous toluene under nitrogen atmosphere. To the reaction mixture was added a solution of tri-*t*-butylphosphine (1 M, 0.42 g, 1.91 mmol) and potassium *t*-butoxide (4.28 g, 38.15 mmol) dropwise slowly. The reaction mixture was stirred for 12 h at 100 °C. The mixture was diluted with dichloromethane and washed with distilled water (150 mL) three times. The organic layer was dried over anhydrous $MgSO_4$ and evaporated in vacuo to give the crude product, which was purified by column chromatography by *n*-hexane. The final product was obtained, a yellow-green powder.

N,N,N′,N′-Tetraphenyl-**SFBF**-5,9-diamine (BD-6DPA). Yield 65%. Mp 270 °C. ^{1}H NMR (500 MHz, $CDCl_3$) δ 8.77–8.76 (d, J = 8.47 Hz, 1H, Ar-CH– naphthalene), 8.23–8.22 (d, J = 8.54 Hz, 1H, Ar-CH–naphthalene), 8.02–8.00 (d, J = 8.37 Hz, 1H, Ar-CH–benzene), 7.69–7.67 (d, J = 7.61 Hz, 2H, Ar-CH–fluorene), 7.61–7.59 (t, J = 8.15 Hz, 1H, Ar-CH–naphthalene), 7.39–7.38 (t, J = 8.00 Hz, 1H, Ar-CH–naphthalene), 7.28–7.26 (t, J = 7.05 Hz, 2H, Ar-CH–fluorene), 7.12–7.10(s, 2H, Ar-CH–benzene), 7.12–7.10 (t, 4H, Ar-CH–benzene), 7.10–7.08 (d, 2H, Ar-CH–fluorene), 6.96–6.94(t, 4H, Ar-CH–benzene), 6.90–6.89(t, 4H, Ar-CH–benzene), 6.89–6.87 (d, 1H, Ar-CH–naphthalene), 6.82–6.81 (d, 4H, Ar-CH–benzene), 6.71–6.69 (d, 1H, Ar-CH–benzene), 6.56–6.56 (d, 1H, Ar-CH–benzene). ^{13}C NMR ($CDCl_3$) δ 151.6, 148.0, 147.9, 147.8, 147.5, 146.8, 142.7, 142.1, 137.1, 135.4, 131.9, 130.8, 129.2, 127.9, 127.8, 127.0, 126.1, 125.7, 124.4, 124.1, 123.9, 123.5, 123.4, 122.9, 121.5, 121.4, 120.3. 119.5, 77.4, 77.2, 76.9, 66.4 ppm.

*N,N′-D*i-(2-naphthyl)-N,N′-diphenyl-**SFBF**-5,9-diamine (BD-6NPA). Yield 62%. Mp 295 °C. ^{1}H NMR (500 MHz, CDCl3) δ 8.80–8.78 (d, J = 8.50 Hz, 1H, Ar-CH- naphthalene), 8.26–8.24 (d, J = 8.54 Hz, 1H, Ar-CH–naphthalene), 8.06–8.05 (d, J = 8.39 Hz, 1H, Ar-CH–benzene), 7.69–7.68 (d, J = 7.62 Hz, 1H, Ar-CH–naphthalene), 7.65–7.63 (d, 2H, Ar-CH–fluorene), 7.65–7.63 (d, 2H, Ar-CH–naphthalene), 7.60–7.57 (t, 1H, Ar-CH–naphthalene), 7.51–7.50 (d, 1H, Ar-CH–naphthalene), 7.43–7.42 (d, 1H, Ar-CH–naphthalene), 7.40–7.38 (d, 2H, Ar-CH–naphthalene), 7.28–7.27 (t, 2H, Ar-CH–fluorene), 7.26–7.24 (t, 2H,

Ar-CH–naphthalene), 7.24–7.21 (d, 2H, Ar-CH–naphthalene), 7.18–7.16 (d, 2H, Ar-CH–naphthalene), 7.16–7.14 (d, 2H, Ar-CH–naphthalene), 7.12–7.10(s, 2H, Ar-CH–benzene), 7.10–7.08(d, 2H, Ar-CH–benzene), 7.08–7.06(d, 1H, Ar-CH–benzene), 7.06–7.04(d, 2H, Ar-CH–benzene), 6.99–6.97 (d, 2H, Ar-CH–fluorene), 6.96–6.94(d, 1H, Ar-CH–benzene), 6.92–6.91(d, 2H, Ar-CH–benzene), 6.90–6.88(d, 1H, Ar-CH–benzene), 6.89–6.87 (d, 1H, Ar-CH–naphthalene), 6.85–6.83(s, 1H, Ar-CH–benzene), 6.73–6.71 (s, 1H, Ar-CH–benzene), 6.63–6.62 (d, 1H, Ar-CH–benzene). ^{13}C NMR ($CDCl_3$) δ 151.7, 148.0, 147.9, 147.7, 147.5, 146.7, 145.7, 145.1, 142.7, 142.1, 137.2, 135.5, 134.4, 131.8, 130.8, 130.1, 129.5, 129.3, 129.1, 128.8, 128.7, 127.9, 127.8, 127.6, 127.1, 127.0, 126.9, 126.3, 126.2, 125.7, 124.6, 124.5, 124.2, 124.1, 124.0, 123.8, 123.5, 123.3, 122.6, 121.8, 121.6, 120.4, 120.0, 119.4, 117.2, 77.4, 77.2, 76.9, 66.4.

N,N′-Diphenyl-*N,N′*-di-*m*-tolyl-**SFBF**-5,9-diamine (BD-6MDPA). Yield 64%. Mp 248 °C. ^{1}H NMR (500 MHz, CDCl3) δ 8.77–8.75 (d, *J* = 8.47 Hz, 1H, Ar-CH–naphthalene), 8.22–8.20 (d, *J* = 8.53 Hz, 1H, Ar-CH–naphthalene), 8.02–8.01 (d, *J* = 8.45 Hz, 1H, Ar-CH–benzene), 7.69–7.67 (d, *J* = 7.60 Hz, 2H, Ar-CH–fluorene), 7.60–7.59 (t, *J* = 8.00 Hz, 1H, Ar-CH–naphthalene), 7.39–7.38 (t, *J* = 7.57 Hz, 1H, Ar-CH–naphthalene), 7.28–7.27 (t, *J* = 7.90 Hz, 2H, Ar-CH–fluorene), 7.12–7.10(s, 2H, Ar-CH–benzene), 7.12–7.10(t, 4H, Ar-CH–benzene), 7.10–7.08 (d, 2H, Ar-CH–fluorene), 7.04–7.02 (d, 2H, Ar-CH–benzene), 6.96–6.94(d, 1H, Ar-CH–benzene), 6.90–6.89(t, 4H, Ar-CH–benzene), 6.89–6.87 (d, 2H, Ar-CH–naphthalene), 6.80–6.78 (d, 2H, Ar-CH–benzene), 6.74–6.72 (d, 2H, Ar-CH–benzene), 6.71–6.68 (d, 2H, Ar-CH–benzene), 6.62–6.60 (d, *J* = 7.92 Hz, 1H, Ar-CH–benzene), 6.57–6.57 (s, 1H, Ar-CH–benzene), 2.08–2.09 (s, 6H, Ar-CH_3). ^{13}C NMR ($CDCl_3$) δ 151.5, 148.1, 147.9, 147.8, 147.5, 147.4, 146.8, 142.7, 142.1, 139.0, 138.8, 136.9, 135.4, 131.9, 130.8, 129.2, 129.0, 128.8, 127.9, 127.8, 126.9, 126.1, 125.7, 124.5, 124.4, 124.1, 123.8, 123.6, 123.3, 123.0, 122.5, 122.1, 121.4, 121.3, 121.1, 120.4, 119.2, 118.6, 77.4, 77.2, 76.9, 66.4, 21.5, 21.4.

N,N′-Diphenyl-*N,N′*-bis(4-(trimethylsilyl)phenyl)-**SFBF**-5,9-diamine (BD-6TMSA). Yield 60%. Mp 256 °C. ^{1}H NMR (500 MHz, $CDCl_3$) δ 8.78–8.76 (d, *J* = 8.50 Hz, 1H, Ar-CH–naphthalene), 8.24–8.23 (d, *J* = 8.53 Hz, 1H, Ar-CH–naphthalene), 8.02–8.00 (d, *J* = 8.42 Hz, 1H, Ar-CH–benzene), 7.69–7.67 (d, *J* = 7.60 Hz, 2H, Ar-CH–fluorene), 7.61–7.59 (t, *J* = 7.38 Hz, 1H, Ar-CH–naphthalene), 7.39–7.38 (t, *J* = 7.70 Hz, 1H, Ar-CH–naphthalene), 7.28–7.27 (t, 2H, Ar-CH–fluorene), 7.24–7.22(d, 2H, Ar-CH–benzene), 7.12–7.10(s, 2H, Ar-CH–benzene), 7.12–7.10(t, 4H, Ar-CH–benzene), 7.10–7.08 (d, 2H, Ar-CH–fluorene), 6.96–6.94(d, 2H, Ar-CH–benzene), 6.90–6.89(d, 2H, Ar-CH–benzene), 6.89–6.87 (d, 1H, Ar-CH–naphthalene), 6.82–6.81 (d, 4H, Ar-CH–benzene), 6.71–6.69 (s, 1H, Ar-CH–benzene), 6.567–6.56 (s, 1H, Ar-CH–benzene), 0.21–0.20 (s, 9H Ar-Si–$(CH_3)_3$), 0.16–0.15 (s, 9H Ar-Si–$(CH_3)_3$). ^{13}C NMR ($CDCl_3$) δ 151.7, 148.5, 148.1, 148.0, 147.8, 147.6, 147.3, 146.6, 142.4, 142.1, 137.3, 135.6, 134.3, 134.2, 133.7, 132.0, 131.8, 130.8, 129.2, 129.1, 127.9, 127.8, 127.0, 126.2, 125.7, 124.4, 124.3, 123.9, 123.8, 123.4, 123.1, 122.7, 121.9, 121.4, 120.3, 120.0, 119.9, 77.4, 77.2, 76.9, 66.4.

2.3. OLED fabrication

A basic device configuration of indium tin oxide(ITO, 150 nm)/*N,N′*-diphenyl-*N,N′*-bis-[4-(phenyl-*m*-tolyl-amino)-phenyl]-biphenyl-4,4′-diamine (DNTPD, 60 nm)/*N,N′*-di(1-naphthyl)-*N,N′*-diphenylbenzidine (α-NPB, 30 nm)/2-methyl-9,10-di(2-naphthyl) anthracene (MADN): dopant (30 nm, x%)/tris(8-hydroxyquinoline)aluminum (Alq_3, 20 nm)/LiF (1 nm)/Al (200 nm) was used for device fabrication. All organic materials except for dopants were deposited at a deposition rate of 1 Å/s. The doping concentration of the dopant materials was varied at 3, 5 and 7%. The devices were encapsulated with a glass lid and a CaO getter after cathode deposition. Current density–voltage-luminance and electroluminescence characteristics of the blue fluorescent OLEDs were measured with a Keithley 2400 source measurement unit and CS 1000 spectroradiometer. Lifetime measurement of the blue OLEDs was carried out at a luminance of 5000 cdm^{-2} at constant current mode.

3. Results and discussion

3.1. Synthesis and characterization

The key intermediate in this synthesis is the introduction of diarylamine substituents into the 5- and 9-position of the **SFBF** by amination reactions, to tune the electro-optical properties of the deep-blue emitting dopant materials. 5,9-Dibromo- **SFBF** (**1**) was prepared by selective bromination of **SFBF** via 5-bromo-**SFBF** using carbon tetrachloride and chloroform solvent as shown in Scheme 1. The dopant materials *N,N,N′,N′*-tetraphenyl-**SFBF**-5,9-diamine (BD-6DPA), *N,N′*-di-(2-naphthyl)-*N,N′*-diphenyl-**SFBF**-5,9-diamine (BD-6NPA), *N,N′*-diphenyl-*N,N′*-dim-tolyl-**SFBF**-5,9-diamine (BD-6MDPA) and *N,N′*-diphenyl-*N,N′*-bis(4-(trimethylsilyl)phenyl)-**SFBF**-5,9-diamine (BD-6TMSA) were prepared by amination reactions of compounds **1** with diphenylamine, *N*-phenyl-2-naphthylamine, 3-methyldiphenylamine and *N*-phenyl-4-(trimethylsilyl)aniline in the presence of a palladium catalyst. The synthetic routes to the four dopant materials are described in Scheme 1. The chemical structures and compositions of the resulting precursor and spiro-compounds were characterized by ^{1}H NMR, ^{13}C NMR, FT-IR and GC–MS.

3.2. Optical properties and energy levels

Table 1 shows the UV–vis absorption and photoluminescence (PL) spectra data of the dopant materials, respectively. The solution absorption maxima of BD-6DPA, BD-6NPA, BD-6MDPA and BD-6TMSA showed at 407, 411, 408 and 407 nm, respectively, whereas the BD-6 series showed at 416, 421, 416 and 413 nm in film. The emission maximum of BD-6DPA, BD-6NPA, BD-6MDPA and BD-6TMSA were located at 478, 464, 468 and 459 nm in solution, respectively, whereas the BD-6 series showed an absorption maximum at 484, 491, 487 and 484 nm in film. The introduction of a diphenylamine group to both the 5- and 9-positions in **SFBF** caused a significant red-shift in

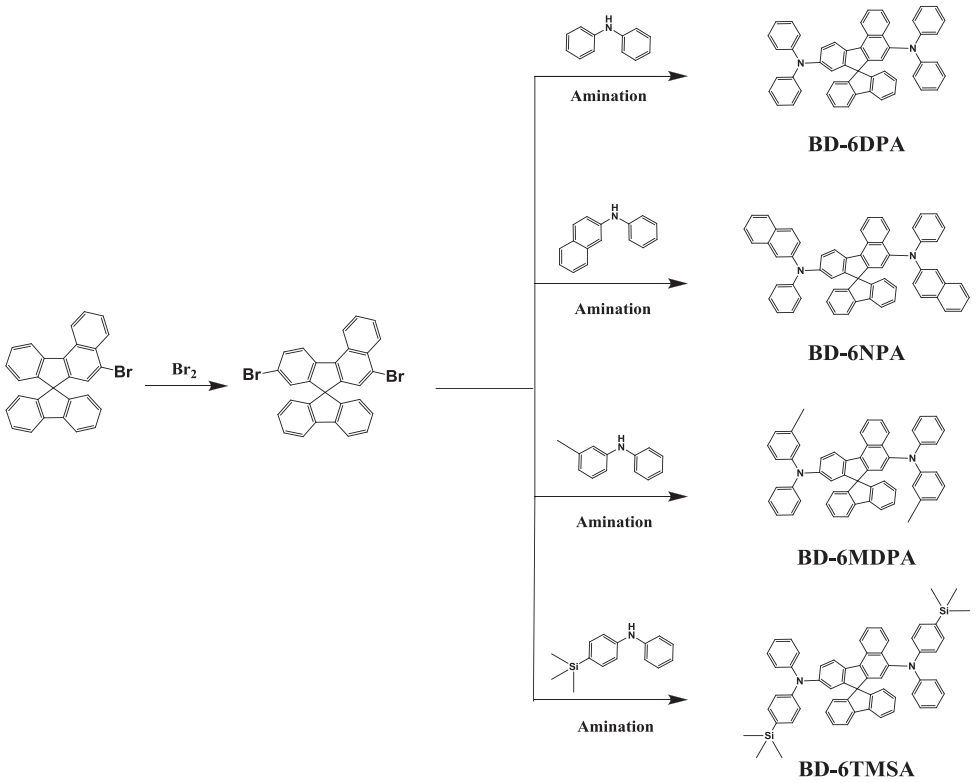

Scheme 1. Synthetic scheme and chemical structure of dopant materials.

Table 1
UV absorption, PL, energy levels and thermal properties of four dopant materials.

Properties	Abs (nm)		PL (nm)		Energy level (eV)		Thermal properties (°C)			Φ_f[a]
Sample	Solution	Film	Solution	Film	HOMO	LUMO	T_g	T_m	T_d	
BD-6DPA	407	416	478	484	5.48	2.77	120	270	429	0.747
BD-6NPA	411	421	464	491	5.44	2.77	154	295	477	0.656
BD-6MDPA	408	416	468	487	5.42	2.70	130	248	436	0.736
BD-6TMSA	407	413	459	484	5.45	2.70	144	256	437	0.672

[a] Fluorescence quantum efficiency, relative to 9,10-diphenylanthracene in cyclohexane (Φ_f = 0.90).

the PL spectrum of BD-6DPA to 478 nm as a result of increased electron donation. The solution fluorescence quantum efficiency (Φ_f) of dopant materials are 0.65 and 0.75, which were determined relative to 9,10-diphenylanthracene in cyclohexane (Φ_f = 0.90). The relatively higher fluorescence quantum efficiency values of BD-6DPA and BD-6MDPA compared to those of BD-6NPA and BD-6TMSA is due to the introduction of the phenyl and tolyl group, which maintains the intermolecular interaction between the emitting materials. A molecular simulation of DPA, NPA, MDPA and TMSA was carried out to understand the physical properties of DPA, NPA, MDPA and TMSA at the molecular level. Density functional theory (DFT) calculations have also been performed to characterize the three-dimensional geometries and the frontier molecular orbital energy levels of DPA, NPA, MDPA and TMSA at the B3LYP/6-31G* level [20] by using the Gaussian 03 program. The optimized structures and the HOMO/LUMO orbitals for DPA, NPA, MDPA and TMS are shown in Fig. 2. Energy gaps for DPA, NPA, MDPA and TMSA were calculated as 3.31 eV, 3.25 eV, 3.31 eV, and 3.30 eV, which corresponded to the absorption wavelengths of 416, 421, 416, and 413 nm, respectively. The calculated geometries of DPA, NPA, MDPA and TMSA in Fig. 1 show that the fluorene and benzofluorene are significantly twisted against each other because of the spiro center, resulting in a non-coplanar structure in each molecule. These geometrical characteristics can effectively prevent intermolecular interactions between π-systems and, thus, suppress molecular recrystallization, which improves the morphological stability of these molecules. Calculated highest occupied molecular orbital (HOMO) and lowest unoccupied molecular orbital (LUMO) density maps of DPA, NPA, MDPA and TMSA are also included in Fig. 1. The electron densities of the HOMOs and

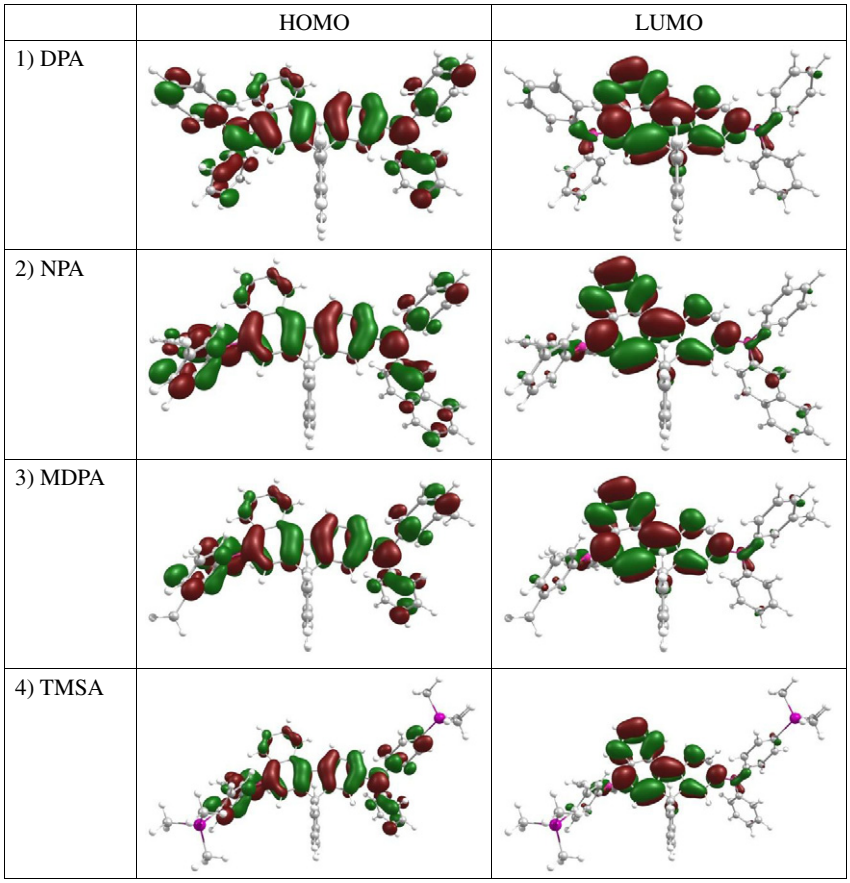

Fig. 1. Molecular simulation results of (a) DPA, (b) NPA, (c) MDPA, and (d) TMSA , showing the HOMO and LUMO orbital distribution (calculated at the DFT/B3LYP/6-31G* for optimization and Time Dependent DFT (TDDFT) using Gaussian 03).

LUMOs are mostly localized on the benzofluorene unit, implying that the absorption and emission processes can only be attributed to the π–π^* transition centered at the benzofluorene unit. As a result, the molecular orbital analysis clearly indicates that the substituents in fluorene unit do not influence the blue emission at all.

3.3. Thermal properties

The thermal properties of the resulting deep-blue emitting materials were characterized with DSC and TGA in a nitrogen atmosphere. The onset decomposition temperatures were 429, 477, 436 and 437 °C for BD-6DPA, BD-6NPA, BD-6MDPA and BD-6TMSA, respectively. Table 1 summarizes the DSC and TGA data for four dopant materials. The purified samples of BD-6DPA, BD-6NPA, BD-6MDPA and BD-6TMSA showed a melting point (T_m) of 270, 295, 248 and 256 °C, respectively. On the second heating, no melting points were observed, even though it was given enough time to cool in air. Once it becomes an amorphous solid, it does not revert to the crystalline state at all. After the sample had cooled to room temperature, a second DSC scan performed at 10 °C/min revealed a high glass transition temperature (T_g) between 120 and 154 °C because of their rigid spiro-type backbone. As a result, the amorphous glassy state of the transparent film of the four dopant materials was a good candidate as an EL material. This suggests that thermal stability was improved significantly by the introduction of various diarylamine groups.

3.4. EL properties

In order to find an optimized dopant concentration, EL spectra were gathered of MADN doped by BD-6 series dopants with different weight concentrations. The emission band increases with the increase of dopant concentration from 3 to 7% by weight. However, it is noted that CIE color coordinates of blue emission did not deviate from deep blue when the doping concentration of BD-6MDPA dopant increases from 5 to 7%. The CIE coordinates of the four devices made of MADN: 7%, 5%, 3%, 0% BD-6MDPA were (0.135, 0.153), (0. 135, 0.156), (0.138, 0.144) and (0.154, 0.164), respectively. It was found that sufficiently deep-blue emission was obtained in the sample with 5% concentration of BD-6MDPA with the CIE coordinates (0.135, 0.156).

OLEDs were fabricated by thermal evaporation onto a cleaned glass substrate precoated with transparent and conductive indium tin oxide (ITO). All the organic layers were grown by thermal evaporation at a deposition rate

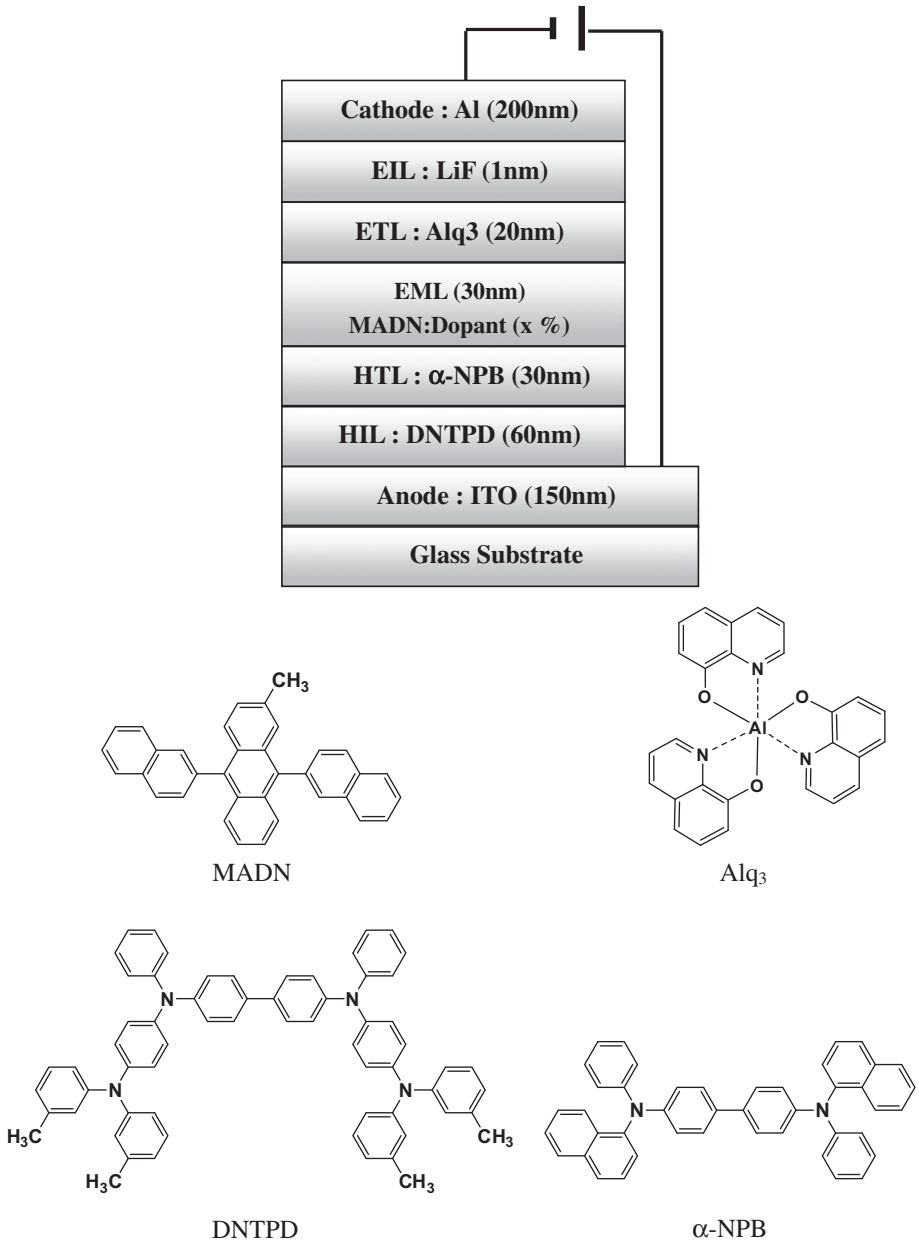

Fig. 2. The device configuration and the chemical structure of the materials used in the devices.

of 1 Å/s. The EL properties of the BD-6DPA, BD-6NPA, BD-6MDPA and BD-6TMSA dopant materials were examined by fabricating multilayer devices with the following configuration: glass ITO anode/HIL/HTL/EML/ETL/EIL/Al cathode. DNTPD was used as the HIL, α-NPB as the HTL, MADN:5% dopant as the EML and Alq3 as the ETL; a 10 Å LiF layer was used as the EIL, as shown in Fig. 2.

Fig. 3 shows the normalized EL spectra of a device composed of MADN doped with BD-6DPA, BD-6NPA, BD-6MDPA and BD-6TMSA at 7 V. All the devices showed intense blue emission in the EL spectra at 465, 463, 462 and 462, respectively. The maximum wavelength of the EL spectra varied significantly according to the dopant material. Based on the EL spectrum, the CIE coordinates of the emitting layer MADN doped with 5% BD-6DPA, BD-6NPA, BD-6MDPA and BD-6TMSA were measured to be (0.135, 0.175), (0.134, 0.168), (0.135, 0.156) and (0.135, 0.151), respectively.

3.5. OLED device properties

Figs. 4 and 5 shows the luminance–voltage and current density–voltage characteristics of the OLEDs with MADN:5% dopant as the EML. The threshold voltage for

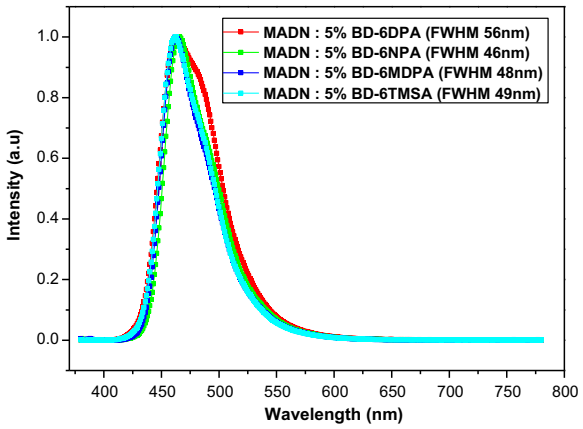

Fig. 3. EL spectra of the devices obtained from MADN host doped with various dopant materials.

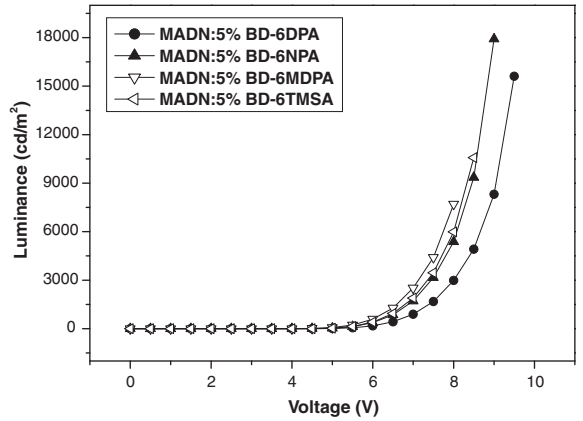

Fig. 4. Luminance–voltage characteristics of the device using MADN:5% dopant.

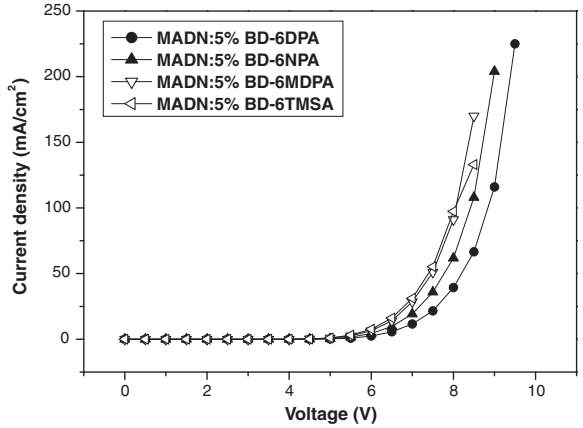

Fig. 5. Current density–voltage characteristics of the device using MADN:5% dopant.

luminescence was about 4.5 V in all the devices. In the case of the device using MADN doped with 5% BD-6MDPA, the maximum brightness of 7699 cdm^{-2} occurs at approximately 8.0 V. Table 2 summarizes the device characteristics at 7 V.

The luminance efficiency of the devices made using MADN:5% dopant were more than 4–6 times higher those of the device without the dopant. This suggests that the dopant is significantly effective in enhancing the EL properties of the spiro-type emitting layer.

The maximum power efficiency of the device obtained from MADN doped with 5% BD-6MDPA was 6.13 l mW^{-1}, which is five times that of the device without the dopant (1.28 l mW^{-1}). The device shows the maximum EQE of 7.95% and the efficiency increased rapidly to a maximum of approximately 8.84 cd A^{-1} at a low current density of 28.50 mA cm^{-2} at 7 V. The holes injected from α-NPB as HTL is transferred to the blue lighting layer and can be trapped to dopant sites. HOMO values of four dopant materials decreased in the order of BD-6DPA (5.48) > BD-6TMSA (5.45) > BD-6NPA (5.44) > BD-6MDPA (5.42). In the case of BD-6DPA having a little difference between the HOMO values of dopant and host materials, the holes from NPB were transferred to ETL as well as EML to causing the loss of holes. However the BD-6MDPA have the large capacity to catch the holes strongly, they minimized the loss of holes to result in the good electroluminescent efficiency. Thus the HOMO level of BD-6MDPA is suitable for holes trapping and the hole transporting properties of the dopant and MADN host is appropriate for balancing holes and electrons in the emitting layer. There was a large difference in EL efficiency between BD-6DPA and BD-6MDPA, even though both materials have almost same PL efficiencies and spectra.

Fig. 6 shows the dependence of luminescence efficiency on the current density of four devices. It can be seen that MADN doped with 5% BD-6NPA shows high efficiency and a small decrease of efficiency as the current density increased from 0 to 175 mA cm^{-2}, *i.e.*, a weak-current-induced fluorescent quenching. It reached a current efficiency of 8.56 cd A^{-1}. This suggests that an exciton is formed and light is emitted at specific thresholds. It should be noted that the efficiencies of these devices remained stable when the current density was increased to 175 mA cm^{-2}. The PL spectrum of MADN overlaps with a major portion of the absorption spectrum of BD-6MDPA. This indicates that BD-6MDPA can effectively accept energy from the host through Förster energy transfer or function as a direct recombination center due to the higher HOMO levels [21]. By using BD-6TMSA as the fluorescent dopant, the PE was successfully enhanced to 5.12 l mW^{-1}, which is four times higher than that of the undoped device. The EQE of OLEDs using BD-6TMSA as the fluorescent dopant with a doping concentration of 5 wt.% was 7.43% with CIE coordinates of (0.135, 0.151).

The device with MADN:5% BD-6-MDPA as EML shows the maximum EQE 8.16% at a current density of 14.0 mA cm^{-2} (6.5 V, 1275 cd m^{-2}) with an luminance efficiency of 9.11 cd A^{-1}, power efficiency of l mW^{-1} and the CIE coordinates of (0.135, 0.157). To our knowledge, this is one of the highest EQE in deep-blue OLEDs. Combined

Table 2
EL properties of the devices obtained from MADN host and four dopant materials.

Devices		MADN			
Properties		BD-6DPA	BD-6NPA	BD-6MDPA	BD-6TMSA
EL at 7 V	λ_{max} (nm)	463	465	462	462
	FWHM (nm)	56	46	48	39
	mA cm^{-2}	11.6	30.3	28.5	31.2
	cd A^{-1}[a]	7.69	8.40	8.84	8.02
	cd A^{-1}[b]	7.79 (7.5 V)	8.56 (6.5 V)	9.11 (6.5 V)	8.11 (6.5 V)
	l mW^{-1}[a]	3.82	4.17	4.39	3.98
	l mW^{-1}[b]	4.43 (5.5 V)	4.61 (6 V)	6.13 (4.5 V)	5.12 (5 V)
	cd m^{-2}	892.6	2544	2520	2503
	CIE-*x*	0.135	0.134	0.135	0.135
	CIE-*y*	0.175	0.168	0.156	0.151
	EQE[a] (%)	6.44	7.2	7.95	7.40
	EQE[b] (%)	6.54 (7.5 V)	7.32 (6.5 V)	8.16 (6.5 V)	7.45 (6.5 V)

[a] Values at 7 V.
[b] Values at a peak.

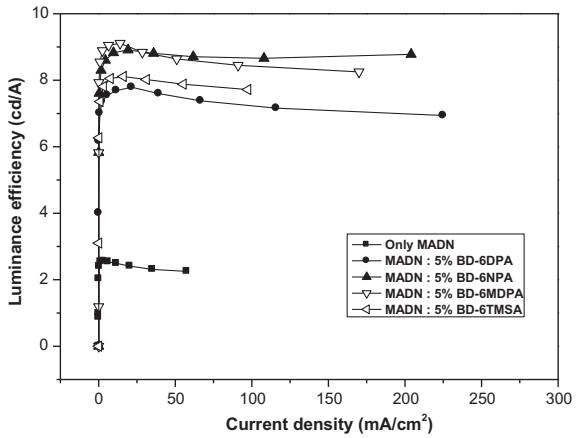

Fig. 6. Efficiency-current density characteristics of the device using MADN:5% dopant.

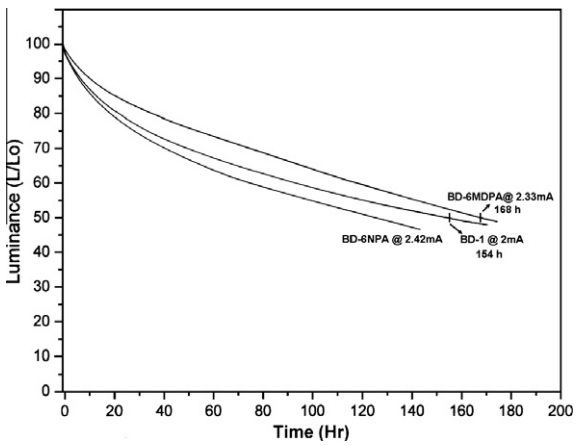

Fig. 7. Lifetime of MADN:5% dopant devices under initial luminance of 5000 cd/m^2 at a constant current.

good efficiency and color purity enables the dopant materials to be a good candidate as a deep-blue emitter for OLEDs.

Among synthesized compounds, the lifetime of BD-6MDPA, which showed the best EL efficiency in this series, was measured as the operational lifetime ($t_{1/2}$) of the blue devices under initial luminance of 5000 cd/m^2 at a constant current. Its lifetime (168 h@2.33 mA) was more than that of MADN:5% BD-1 (154 h@2 mA) as shown in Fig. 7.

4. Conclusion

A series of new deep-blue light emitting spiro-type dopant materials (BD-6DPA, BD-6NPA, BD-6MDPA and BD-6TMSA) were successfully prepared by amination reactions of 5,9-dibromo-**SFBF** with various diarylamines. When the device configuration of ITO/DNTPD/NPB/MADN:dopant/Alq_3/LiF/Al was constructed, the EL emissions of the devices (doped with 5% BD-6MDPA) are observed at 463 nm. In optimized structures, the device obtained using MADN:5% BD-6MDPA had greatest resulted in high performance OLEDs with a high external quantum efficiency of 8.16% and deep-blue emission, having CIE coordinates (0.135, 0/156). According to these characteristics, these deep-blue emitting materials have sufficient potential for display applications.

Acknowledgement

This research was supported by WCU (World Class University) program through the National Research Foundation of Korea funded by the Ministry of Education, Science and Technology (R31-10069).

References

[1] C.W. Tang, S.A. VanSlyke, Appl. Phys. Lett. 51 (1987) 913–915;
L.S. Hung, C.H. Chen, Mater. Sci. Eng. 39 (2002) 143;
U. Mitschke, P. Bäuerle, J. Mater. Chem. 10 (2000) 1471;
Y. Shirota, J. Mater. Chem. 10 (2000) 1.
[2] C.H. Chen, C.W. Tang, J. Shi, K.P. Klubek, Thin Solid Films 363 (2000) 327;
P. Wang, Z. Hong, Z. Xie, S. Tong, O. Wong, C.S. Lee, N. Wong, L. Hung, S. Lee, Chem. Commun. 14 (2003) 1664;
G. Cheng, Y.F. Zhang, Y. Zhao, S.Y. Liu, S. Tang, Y.G. Ma, Appl. Phys. Lett. 87 (2005) 151905;
W.J. Shen, R. Dodda, C.C. Wu, F. Wu, T.H. Liu, C.H. Chen, C.F. Shu, Chem. Mater. 16 (2004) 930;

S. Tao, Z. Hong, Z. Peng, W. Ju, X. Zhang, P. Wang, S. Wu, S. Lee, Chem. Phys. Lett. 397 (2004) 1;
H.T. Shih, C.H. Lin, H.H. Shin, C.H. Cheng, Adv. Mater. 14 (2002) 1409;
K. Danel, T.H. Huang, J.T. Lin, Y.T. Tao, C.H. Chuen, Chem. Mater. 14 (2002) 3860;
Y.H. Kim, H.C. Jeong, S.H. Kim, K. Yang, S.K. Kwon, Adv. Funct. Mater. 15 (2005) 1799;
C. Huang, C.G. Zhen, S.P. Su, K.P. Loh, Z.K. Chen, Org. Lett. 7 (2005) 391.

[3] Y. Xiong, W. Xu, C. Li, B. Liang, L. Zhao, J. Peng, Y. Cao, J. Wang, Org. Electron. 9 (2008) 533.

[4] A. Kadashchuk, A. Vakhnin, Yu. Skryshevski, V.I. Arkhipov, E.V. Emelianova, H. Bässler, Chem. Phys. 291 (2003) 243.

[5] S. Tokito, H. Tanaka, K. Noda, A. Okada, Y. Taga, Appl. Phys. Lett. 70 (1997) 1929.

[6] M.T. Lee, H.H. Chen, C.H. Tsai, C.H. Liao, C.H. Chen, Appl. Phys. Lett. 85 (2004) 3301.

[7] Q. Pei, Y. Yang, J. Am. Chem. Soc. 118 (1996) 7416;
Y. Ohmori, M. Uchida, K. Muro, K. Yoshino, Jpn. J. Appl. Phys. 30 (1991) L1941.

[8] S.M. Kelly, Flat Panel Displays: Advanced Organic Materials, Royal Society of Chemistry, Cambridge, UK, 2000.

[9] P.I.S. Tobat, S. Till, S. Achim, F.L. Thomas, S. Josef, Chem. Rev. 107 (2007) 1011;
H. Xiao, H. Shen, Y. Lin, J. Su, Dyes Pigm. 73 (2007) 224;
J. Pei, J. Ni, X.H. Zhou, X.Y. Cao, Y.H. Lai, J. Org. Chem. 67 (2002) 4924;
J.H. Fournier, T. Maris, J.D. Wuest, J. Org. Chem. 69 (2004) 1762;
H. Lee, J. Oh, H.Y. Chu, J.I. Lee, S.H. Kim, Y.S. Yang, G.H. Kim, L.-M. Do, T. Zyung, J. Lee, Y. Park, Tetrahedron 59 (2003) 2773.

[10] C.T. Chen, C.H. Chien, J. Am. Chem. Soc. 128 (2006) 10992;
K.T. Wang, C.L. Wang, Org. Lett. 3 (2001) 2285.

[11] F. Milota, C. Warmuth, A. Tortschanoff, J. Sperling, T. Fuhrmann, J. Salbeck, H.F. Kauffmann, Synth. Met. 121 (2001) 1497.

[12] V. Prelog, D. Bedekovic, Helv. Chim. Acta 62 (1979) 2285;
N. Harada, H. Ono, T. Nishiwaki, H. Uda, Chem. Commun. 24 (1991) 1753;
V. Alcazar, F. Diederich, Angew. Chem. 104 (1992) 1503;
T. Spehr, A. Siebert, T. Fuhrmann-Lieker, S. Salbeck, T. Rabe, T. Riedl, H.H. Johannes, W. Kowalsky, J. Wang, T. Weimann, P. Hinze, Appl. Phys. Lett. 87 (2005) 161103.

[13] K.T. Wong, Y.L. Liao, Y.T. Lin, H.C. Su, C.C. Wu, Org. Lett. 7 (2005) 5131.

[14] D. Gebeyehu, K. Walzer, G. He, M. Pfeiffer, K. Leo, J. Brandt, A. Gerhard, P. Stoessel, H. Vestweber, Synth. Met. 148 (2005) 205.

[15] Y.H. Kim, D.C. Shin, S.H. Kim, C.H. Ko, H.S. Yu, Y.S. Chae, S.K. Kwon, Adv. Mater. 13 (2001) 1690.

[16] R. Pudzich, J. Salbeck, Synth. Met. 138 (2003) 21.

[17] S. Tao, Z. Peng, X. Zhang, P. Wang, C.S. Lee, S.T. Lee, Adv. Funct. Mater. 15 (2005) 1716–1721.

[18] D. Horhant, J.J. Liang, M. Virboul, C. Poriel, G. Alcaraz, J. Rault-Berthelot, Org. Lett. 8 (2006) 257.

[19] S.O. Jeon, Y.M. Jeon, J.W. Kim, C.W. Lee, M.S. Gong, Org. Electron. 9 (2008) 522;
S.O. Jeon, Y.M. Jeon, J.W. Kim, C.W. Lee, M.S. Gong, Synth. Met. 159 (2009) 1147;
S. Hamai, F. Hirayama, J. Phys. Chem. 87 (1983) 83;
K.S. Kim, H.S. Lee, Y.M. Jeon, J.W. Kim, C.W. Lee, M.S. Gong, Dyes Pigm. 81 (2009) 174;
Y.M. Jeon, J.W. Kim, C.W. Lee, M.S. Gong, Dyes Pigm. 83 (2009) 66;
S.O. Jeon, Y.M. Jeon, J.W. Kim, C.W. Lee, M.S. Gong, Synth. Met. 159 (2009) 1147;
K.S. Kim, Y.M. Jeon, H.S. Lee, J.W. Kim, C.W. Lee, M.S. Gong, Synth. Met. 158 (2008) 870;
K.S. Kim, Y.M. Jeon, J.W. Kim, C.W. Lee, M.S. Gong, Org. Electron. 9 (2008) 797;
J.H. Kim, Y.M. Jeon, J.G. Jang, S. Ryu, H.J. Chang, C.W. Lee, J.W. Kim, M.S. Gong, Bull. Korean Chem. Soc. 30 (2009) 647;
S.O. Jeon, H.S. Lee, Y.M. Jeon, J.W. Kim, C.W. Lee, M.S. Gong, Bull. Korean Chem. Soc. 30 (2009) 863.

[20] M.J. Frisch et al., GAUSSIAN 03, Revision B.05, Gaussian, Inc., Pittsburgh, PA, 2003.

[21] S.J. Lee, J.S. Park, K.J. Yoon, Y.I. Kim, S.H. Jin, S.K. Kang, Y.S. Gal, S.W. Kang, J.Y. Lee, J.W. Kim, S.H. Lee, H.D. Park, J.J. Kim, Adv. Funct. Mater. 18 (2008) 3922.

[22] M.T. Lee, C.H. Liao, C.H. Tsai, C.H. Chen, Adv. Mater. 17 (2005) 2493.

[23] W. Norbert, A. Mitzel, S.H. Klaus, Chem. Ber. 127 (1994) 841.